The fate of early Mars' lost water: The role of serpentinization

Eric Chassefière, Benoit Langlais, Yoann Quesnel, François Leblanc

The fate of early Mars' lost water: The role of serpentinization

Eric Chassefière,[1,2] Benoit Langlais,[3] Yoann Quesnel,[4] and François Leblanc[5]

Received 4 December 2012; revised 30 April 2013; accepted 1 May 2013; published 30 May 2013.

[1] The fate of water which was present on early Mars remains enigmatic. We propose a simple model based on serpentinization, a hydrothermal alteration process which may produce magnetite and store water. Our model invokes serpentinization during about 500 to 800 Myr, while a dynamo is active, which may have continued after the formation of the crustal dichotomy. We show that the present magnetic field measured by Mars Global Surveyor in the southern hemisphere is consistent with a ~500 m thick Global Equivalent Layer (GEL) of water trapped in serpentine. Serpentinization results in the release of H_2. The released H atoms are lost to space through thermal escape, increasing the D/H ratio in water reservoirs exchanging with atmosphere. We show that the value of the D/H ratio in the present atmosphere (~5) is also consistent with the serpentinization of a ~500 m thick water GEL. We reassess the role of nonthermal escape in removing water from the planet. By considering an updated solar wind-ionosphere interaction representation, we show that the contribution of oxygen escape to H isotopic fractionation is negligible. Our results suggest that significant amounts of water (up to a ~330–1030 m thick GEL) present at the surface during the Noachian, similar to the quantity inferred from the morphological analysis of valley networks, could be stored today in subsurface serpentine.

Citation: Chassefière, E., B. Langlais, Y. Quesnel, and F. Leblanc (2013), The fate of early Mars' lost water: The role of serpentinization, *J. Geophys. Res. Planets*, *118*, 1123–1134, doi:10.1002/jgre.20089.

1. Introduction

[2] Like Earth, Mars has been endowed with large amounts of water during accretion, equivalent to the content of several terrestrial oceans, corresponding to a several 10 km thick Global Equivalent Layer (GEL) [*Raymond et al*., 2006]. The present inventory of observable water on Mars is quite smaller, although not precisely known. The total water content of the two perennial polar caps corresponds to a GEL of 16 m [*Smith et al*., 2001], and the ice deposits sequestered in the Dorsa Argentea Formation (DAF), near the south polar cap, may have represented ~15 m in the past [*Head and Pratt*, 2001]. Nevertheless, only a fraction of the initial water could remain today in DAF reservoir, corresponding to ~5–7.5 m. Based on Mars Advanced Radar for Subsurface and Ionosphere Sounding radar experiment on board Mars Express, high dielectric values were found in midlatitude belts (20–40°), and lower ones at both polar and equatorial latitudes. These were interpreted in terms of water-ice presence within the regolith, possibly accounting for 7 m GEL [*Mouginot et al*., 2010]. The present inventory of water in the known surface or subsurface reservoirs is therefore in the range from ~20 to 30 m.

[3] The mega-regolith capacity is large, with up to ~500 m GEL potentially trapped in the cryosphere, and hypothetically several additional hundreds of meters (up to ~500 m) of groundwater surviving at depth below the cryosphere [*Clifford et al*., 2010]. A ~500 m thick GEL is generally assumed to be required to explain the formation of outflow channels [*Carr*, 1987], and most of this water could be trapped today as water ice, and possibly deep liquid water, in the subsurface, and also possibly under the form of hydrated minerals.

[4] The presence of hydrated minerals at the surface of Mars [*Bibring et al*., 2006; *Mustard et al*., 2008] suggests that hydration processes have been active. Such minerals may have been formed, either at the surface of Mars during the Noachian, when liquid water was flowing at the surface of the planet, or in the subsurface by aqueous alteration of subsurface rocks, and possibly by impacts able to provide subsurface water to the impacted material [*Bibring et al*., 2006]. Existing geochemical model calculations show that hydrothermal hydration of Martian crust is an efficient process [*Griffith and Shock*, 1997]. According to this last study, water storage via hydrous minerals can account for ~ wt 5% of crustal rocks. Clays observed in outcrops of the Noachian crust have been recently suggested to have formed by precipitation of water-rich fluids in subsurface magmatic systems [*Meunier et al*., 2012].

[5] A particular hydration process occurring in Earth's crust is serpentinization, which generates H_2 from the reaction of

[1]Laboratoire IDES, UMR 8148, Université Paris-Sud, Orsay, France.
[2]CNRS, Orsay, France.
[3]Laboratoire de Planétologie et Géodynamique de Nantes, UMR 6112, CNRS, Université de Nantes, Nantes, France.
[4]CNRS, IRD, CEREGE UM34Aix-Marseille Université, Aix-en-Provence, France.
[5]Laboratoire Atmosphères Milieux Observations Spatiales/IPSL, CNRS-UVSQ, Université Pierre et Marie Curie, Paris, France.

Corresponding author: E. Chassefière, IDES, Université Paris-Sud, CNRS, Bât. 504, Orsay, F-6 91405, France. (eric.chassefiere@u-psud.fr)

2169-9097/13/10.1002/jgre.20089

water with ferrous iron derived from minerals, primarily ultramafic rocks [*McCollom and Back*, 2009]. In the reaction, ferrous iron is oxidized by the water to ferric iron, which typically precipitates as magnetite, while hydrogen from water is reduced to H_2. Iron oxidation is accompanied by the storage of a large number of water molecules in serpentine, a hydrated mineral which has been recently observed on Mars [*Ehlmann et al*., 2009]. Based on an analysis of the present Mars' D/H ratio, a water GEL of up to ~300–400 m thickness may have been stored in crustal serpentine on early Mars [*Chassefière and Leblanc*, 2011a, referred to as CL11 in this paper]. Serpentinization of the southern crust has been suggested to be at the origin of both the crustal dichotomy and the strong remanent magnetic field of old southern terrains [*Quesnel et al*., 2009, referred to as Q09 in this paper].

[6] All these reservoirs could have exchanged with each other, as well as with atmosphere and polar caps, at the occasion of magmatic and hydrothermal events that are expected to have occurred at Noachian and Hesperian times, and to a lesser extent during the Amazonian, and could contain up to a 1 km or so thick GEL of water. Nevertheless, on the present Mars, surface and close subsurface reservoirs could not anymore exchange with deeper reservoirs due to the declining internal activity of the planet.

[7] Pyroxenes and olivines have been detected in substantial amounts at the surface of Mars [*Bibring et al*., 2006; *Koeppen and Hamilton*, 2008]. Serpentine has been recently observed in the Nili Fossae region [*Ehlmann et al*., 2008] and in Valles Marineris areas [*Quantin et al*., 2012] associated with alteration minerals. From existing bulk composition models, the MgO/(MgO + FeO) ratio in the Martian mantle could be ~0.75, smaller than the Earth mantle value of ~0.90 [*Longhi et al*., 1992]. Assuming for instance a typical magnesium content of 75% (Forsterite Fo75: $(Mg_{0.75}Fe_{0.25})_2SiO_4$) equal to the expected magnesium content of the bulk mantle, a typical serpentinization reaction can be expressed as [*Oze and Sharma*, 2007; Q09]:

$$Mg_{1.5}Fe_{0.5}SiO_4 + 7/6H_2O \rightarrow 1/2Mg_3Si_2O_5(OH)_4 + 1/6Fe_3O_4 + 1/6H_2 \quad (1)$$

[8] A number of other reactions are considered in the study below and are discussed in section 2 and in the Appendix. All these reactions produce chrysotile $Mg_3Si_2O_5(OH)_4$ and magnetite Fe_3O_4. For one water molecule lost through iron oxidation through reaction (1), six molecules are involved in the hydration of olivine and trapped in serpentine. As a consequence, one H_2 molecule released to the atmosphere is the counterpart of six H_2O molecules stored in the crust; this amount translating in 24 H_2O molecules if the released molecule is CH_4 instead of H_2 (CL11). Once released, CH_4 is converted to H_2 and CO_2 through oxidation. The release of H_2 and/or CH_4 therefore results in an increase of the atmospheric H_2 buffer content, followed by an increase of the thermal escape flux of hydrogen, which is nearly proportional to the H_2 mixing ratio (CL11). In this way, the hydrogen released by the oxidation of the deep crust is lost to space, as imposed by the regulation of the redox state of the atmosphere by the balance between the O and H loss fluxes [*Liu and Donahue*, 1976]. Crustal oxidation through serpentinization therefore results in the escape of the H atoms released by oxidation (under the form of H_2 and CH_4, and possibly other hydrocarbons), with subsequent isotopic fractionation of H. A highly serpentinized crust is expected to result in a high D/H ratio, as observed in Mars' atmosphere.

[9] The D/H ratio in Mars' atmosphere is 5.2 times higher than the corresponding ratio in the Earth's ocean [*Owen et al*., 1988; *Bjoraker et al*., 1989]. This enrichment is interpreted as the result of the fractionation of hydrogen by thermal escape [*Owen et al*., 1988]. Indeed, the thermal escape of deuterium is quite small with respect to the hydrogen escape rate [*Krasnopolsky*, 2002]. Assuming that large quantities of hydrogen have escaped to space by thermal escape, most of the corresponding deuterium is still on the planet today under the form of HDO in Mars water reservoirs.

[10] The main goal of the present paper is to reassess the hypothesis that serpentinization may have played a major role in removing a several hundred meters thick GEL of water, by using the magnetization of ancient Martian terrains as an additional constraint on the serpentinization rate (Q09). First (section 2), assuming that the magnetization of the southern crust is due to serpentinization, we estimate the amount of water required to have been trapped in serpentine to explain remanent magnetic field observations. We describe (section 3) how recent models of Mars solar wind interactions show that an increased solar activity might result in a higher planetopause inducing nonthermal escape rates lower than previously estimated [*Chassefière et al*., 2007]. Such low escape rates are unable to explain the removal of significant amounts of H_2O (and CO_2) through O (and C) escape, since the late Noachian/Hesperian transition. In section 4, we calculate the expected D/H ratio induced by serpentinization, nonthermal escape, and sulfur oxidation. We then examine if consistent solutions, in terms of both crustal magnetization and hydrogen isotopic fractionation, exist and propose a plausible estimate of the amount of water trapped in serpentine. The implications of our results for the early history of Mars are discussed in the final section.

2. Modeling of Serpentinization and Consequences for Crustal Magnetization and Hydrogen Isotopic Fractionation

[11] The measured present-day magnetic field of Mars is related to both ancient dynamo processes (and notably its strength and time-variability, e.g., *Amit et al*. [2011]) and to magnetization processes (defining the efficiency or ability for a given rock to acquire and eventually keep a magnetization). It is difficult to make a clear distinction of what contributed more to the current magnetization and is further complicated by the demagnetization processes which could have occurred since.

[12] Having these limits in mind, it is, however, possible to estimate what the present magnetization in the Martian lithosphere is. *Parker* [2003] computed the minimum magnetization required to locally explain the very intense magnetic field observed above the Martian surface. Assuming that this magnetization is restricted to either a 25 or a 50 km thick layer, ideal body theory predicts that it has to exceed 8.31 or 4.76 A/m, respectively. *Langlais et al*. [2004] computed a global model of the magnetization, using an Equivalent Source Dipole (ESD) method. Assuming that the magnetization is restricted to a 40 km thick layer and that this layer can be described by 4840 equidistant bodies, then magnetization

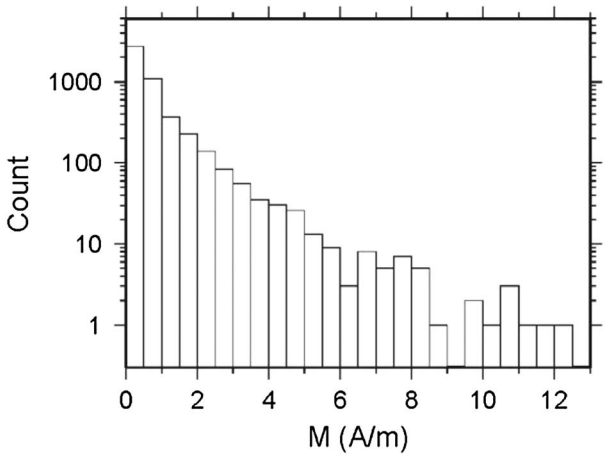

Figure 1. Distribution of magnetization strengths in the equivalent source dipole model of *Langlais et al*. [2004].

intensity ranges between 0 and 12.25 A/m. We show in Figure 1 the histogram of the magnetization. Most of the ESD are found with magnetization lower than 1 A/m, and only 20% possess larger values. A very limited number reaches extreme values, with only 10 ESD showing magnetization larger than 10 A/m. Assuming a very conservative error of 1 A/m in the ESD model (mainly because of the nonuniqueness of the solution), the observed Martian magnetic field can be explained by 20% of its surface being magnetized.

[13] This ESD model actually reflects the vertically integrated magnetization, the product of the magnetization M by the thickness h. A similar magnetic field can be predicted at observation altitude by this constant thickness model and by a constant magnetization model with varying thickness, assuming $h \times M$ constant. We can therefore convert this ESD magnetization model into a magnetized thickness model, assuming a constant magnetization.

[14] In order to do so, we need to define what would be the magnetization intensity associated with the serpentinization reaction. Several factors affect the serpentinization kinematics and degree. In the presence of water, first-order ones are the nature of the initial material and especially the grain size, and the temperature [e.g., *Malvoisin et al*., 2012]. The degree of serpentinization depends on these factors and affects also the resulting magnetization. Serpentinization is favored by small olivine grain sizes and a temperature close to 300°C. In the nature, serpentinized peridodite samples commonly show serpentinization degrees between 40% and 100% [e.g., *Oufi et al*., 2002]. Small grain size also favors the creation of chrysotile instead of lizardite, in which iron can be more easily trapped. Above 75% lizardite is destabilized to form more chrysotile and magnetite [*O'Hanley and Dyar*, 1993, 1998]. Because we seek reactions producing chrysotile rather than lizardite, we assume small olivine grain sizes, which can lead to large serpentinization degree (>90%) [*Malvoisin et al*., 2012].

[15] The amount of magnesium is also critical. For example, for a magnesium content lower than 50%, serpentinization is thermodynamically inefficient [*Oze and Sharma*, 2007]. As already stated, the MgO/(MgO + FeO) ratio (or Mg number) in the Martian mantle could be ~0.75 [*Longhi et al*., 1992]. The uppermost 1000 km of the mantle are likely dominated by olivine and orthopyroxene. Like terrestrial mantle olivine (Fo90), this magnesium-rich olivine (Fo75) falls within the range of magnesium content (Fo50–Fo100) where serpentinization is thermodynamically possible, and may proceed at significant kinetic rates, even at low temperatures [*Oze and Sharma*, 2007].

[16] The bulk Mg-rich olivine on Mars is constrained to Fo ~ 60–90 by estimates based on Martian meteorites [see *Koeppen and Hamilton*, 2008, and references therein] in good agreement with mantle bulk composition models, although Mg-poor olivines (Fo ~ 0–50) are found in some SNC meteorites [see *Taylor et al*., 2002, Figure 10]. Spectral measurements made by the Mars Global Surveyor Thermal Emission Spectrometer (TES) show that the confidently identified Fo68 spectral end-member is abundant at the surface of Mars, but olivine with lower magnesium content (end-members from Fo18 to Fo53) are also present. The combination of mantle composition modeling, Martian meteorite analysis, and spectral observation of Mars surface therefore provides a self-consistent picture, with an upper mantle consisting in an average of Fo ~ 75 and an upper crust olivine with a more extended range magnesium content (Fo ~ 18–91).

[17] In the following and for simplicity, we assume an Mg number equal to 75, with four possible reactions as shown in Table 1. Other reactions are given in Table A1 of Appendix A. The given magnetization intensity corresponds to those attained under a magnetizing field of 50,000 nT [see Q09, equations (4)–(6)]. Assuming Fo75 (but also enstatite, as in section A1), these reactions produce magnetite, with an estimated magnetization ranging between 13.7 and 15.6 A/m.

[18] In the following, we assume that the serpentinization degree is equal to 90%. Under a 50,000 magnetic field,

Table 1. Serpentinization Reactions Considered in This Study, With Associated Magnetization Intensities and Ingoing H_2O to Outgoing H_2 Ratios

ID	Reactions of Serpentinization[a]	Magnetization ($A\,m^{-1}$)[b]	$r = H_2O_{in}/H_{2out}$[c]
1	$6Fo75 + 7H_2O = 3Ch + Mt + H_2$	14.4	7
2	$24Fo75 + 0.75Fs + 28.5H_2O = 12Ch + 4.5Mt + 1.5Q + 4.5H_2$	15.6	6.3
3	$15Fo75 + 6En65 + 24.1H_2O = 10.1Ch + 3.9Mt + 6.8Q + 3.9H_2$	14.6	6.2
4	$6Fo75 + 3En70 + 10.4H_2O = 4.4Ch + 1.6Mt + 3.2Q + 1.6H_2$	13.7	6.5

[a]Abbreviations: Fo, Forsterite ($(Mg,Fe)2S_iO_4$); Ch, Chrysotile ($Mg_3Si_2O_5(OH)_4$); Mt, Magnetite (Fe_3O_4); En, Enstatite ($(Mg,Fe)_2Si_2O_6$); Q, Quartz (SiO_2); Fs, Ferrosillite ($Fe_2Si_2O_6$). Indices in Fo and En correspond to the magnesium content relative to iron (e.g., Fo75 means $(Mg_{0.75}Fe_{0.25})_2SiO_4$).

[b]Magnetization intensities are calculated via volume percentage of magnetite, magnetic susceptibility, and assuming a surface magnetic field during magnetization of 50,000 nT.

[c]Ratio between ingoing H_2O molecules and outgoing H_2 molecules.

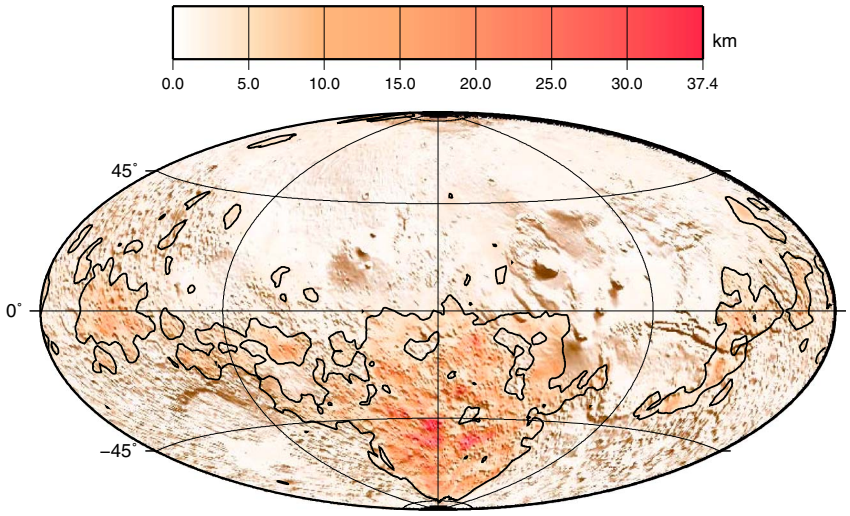

Figure 2. Thickness of the magnetized layer required to explain the magnetic field of Mars, assuming a chemical remanent magnetization due to a 90% serpentinization rate. Contour denotes the 3.05 km thickness conservative limit.

alteration of Fo75 leads to a magnetization of on average 14.6 A/m. This is scaled to 13.1 for a 90% serpentinization degree. This number is used to convert the magnetization model into a model of the serpentinized thickness. To explain the maximum estimated magnetization of 12.25 A/m (for a 40 km thick layer, see *Langlais et al*. [2004]), a maximum thickness of 37.4 km is required. This result is compatible with the estimates of Q09 who computed the thickness of the to-be-serpentinized layer in order to explain both the topographic and magnetic dichotomy of the southern Martian hemisphere. The magnetization model (constant magnetized thickness) is converted into a thickness model (constant magnetization), using these figures (13.1 A/m, maximum thickness 37.4 km). The resulting model is shown in Figure 2. Based on this model, the total volume required to explain the magnetic field observations is 12051 km (total thickness) times 29900 km^2 (the average surface of one ESD), or 3.60×10^8 km^3. This is equivalent to a GEL of 2.49 km of serpentinized material.

[19] In Figure 2, we also highlight the 3.05 km thickness isocontour. This limit corresponds to the conservative magnetization lower bound of 1 A/m. Taking into account this limit, the cumulative thickness of the serpentinized layer becomes 7223 km, equivalent to a 1.49 km serpentinized GEL.

[20] The molar mass of chrysotile $Mg_3Si_2O_5(OH)_4$ is 277 g. Because two molecules of H_2O are trapped in one chrysotile molecule, 1 mol of chrysotile contains 36 g of water. The density of chrysotile is 2.53 g cm^{-3}. The density of water in chrysotile is therefore $2.53 \times 36/277 = 0.33$ g cm^{-3}. A 1.49 km thick serpentinized GEL is therefore equivalent to a 0.49 km thick water GEL. This value is obtained by using the conservative estimate of the thickness of the serpentinized layer. Using a thickness of 2.49 km, the thickness of the involved water GEL is 0.82 km. The quantity of water trapped in serpentine is therefore in the range from 490 to 820 m.

[21] Before calculating the D/H ratio generated by oxygen loss, in particular due to iron oxidation in the course of serpentinization, it is necessary to precisely assess the question of the oxygen escape and related loss. The following section provides an estimate, based on most recent models, of both oxygen and carbon escape.

3. Estimates of the Cumulated Loss Rates of O and C by Nonthermal Escape

[22] Any estimate of the cumulated amounts of C and O atoms lost to space from Mars' atmosphere during Mars' history suffers from the large and numerous uncertainties on the different processes that should lead to atmospheric escapes [*Chassefière and Leblanc*, 2004; *Chassefière et al*., 2007]. This is particularly true when dealing with the nonthermal atmospheric escape channels that should dominate the water and CO_2 escapes during the last 4 Gyr. As an example, ion escape rates at present solar activity (minimum and maximum) are still debated after Phobos-2 and Mars Express missions [*Lundin et al*., 1989, 2008]. However, observations of Mars' atmospheric ion escape suggest a significant dependency with respect to solar wind dynamic pressure and a less obvious dependency with respect to EUV/UV flux [*Nilsson et al*., 2011]. Such information is crucial to derive cumulated amounts of C and O atoms loss along Mars' history. Indeed, it is the dependency of these escaping rates with respect to solar photon activity, solar wind conditions, and atmospheric structures and composition which drives the fate of Mars' atmospheric escape on solar system evolution timescale.

[23] Unfortunately, because only relatively limited observations are presently available at various solar conditions, any actual extrapolation to past conditions of Mars' atmospheric escape depends on our understanding of the processes at the origin of Mars' present escape. In the following, we present two estimates of atmospheric escape due to different processes described in *Chassefière and Leblanc* [2004] and *Chassefière et al*. [2007] and in a more recent set of papers [*Chassefière and Leblanc*, 2011b; CL11]. By doing so, we wish to highlight how our understanding of Mars' solar wind and photon fluxes interaction evolved and impacted our estimate of Mars' cumulated atmospheric escape.

[24] In Figure 3, the two panels on the left describe *Chassefière and Leblanc*'s [2004] scenario of evolution of the

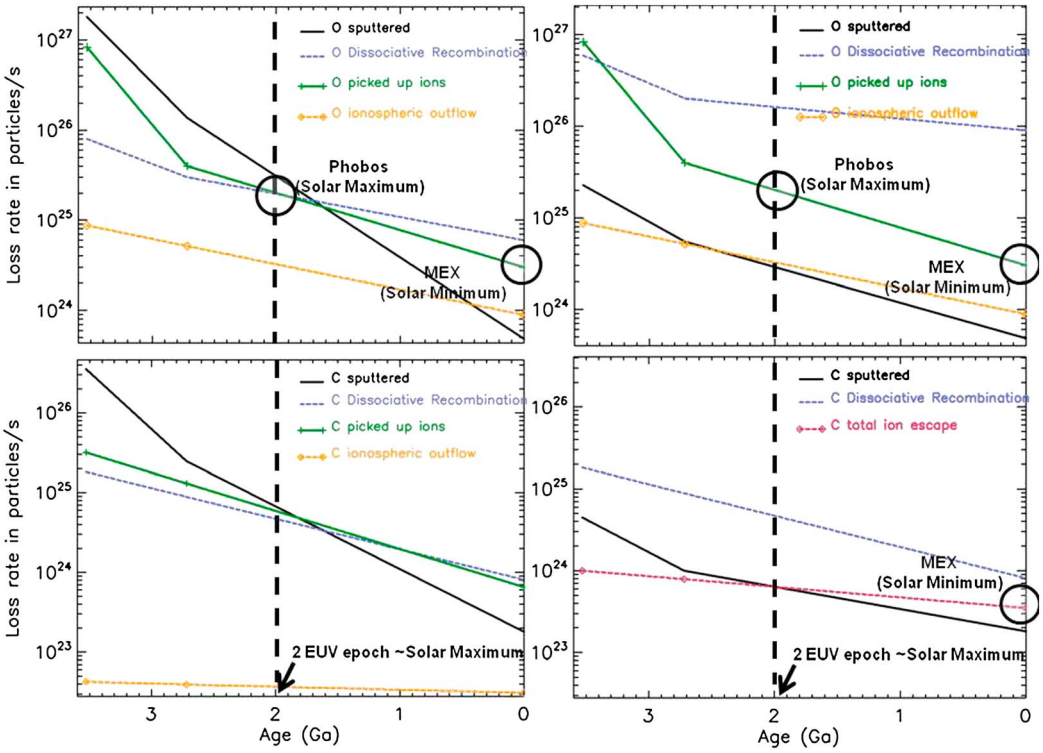

Figure 3. Time evolution of the loss rate of the (upper panel) O and (lower panel) C atmospheric Martian atoms along Mars' history following the different processes thought to act on Mars' atmosphere. (dark solid line) O atoms sputtered from Mars' atmosphere. (green solid line) Picked up ion rates. (dashed blue line) O atoms ejected from Mars' atmosphere by photodissociative recombination. (orange dashed line) Ionospheric outflows. (left panel) Based on *Chassefière and Leblanc* [2004]. (right panel) Based on CL11 and *Chassefière and Leblanc* [2011b].

different processes of escape along Mars' history. To calculate such an evolution, it was supposed that the main driver of Mars' atmospheric escape was the UV/EUV flux intensity [*Luhmann et al*., 1992]. Therefore, estimates of the O and C escape rates were made at various solar activity epochs, namely at 1 time the EUV flux at present epoch solar minimum, 2 times the present EUV for present solar maximum conditions, corresponding to the effective flux 2.55 Gyr ago [*Chassefière et al*., 2007], 3 times the present EUV flux for an epoch 3.5 Gyr ago, and 6 times the present EUV flux, that is 3.9 Gyr ago. Such an extrapolation back in time is usually limited to a time when it is thought that major events occurred at the surface of Mars, including Tharsis formation and the late heavy bombardment [*Bibring et al*., 2006]. The presence (or its disappearance) of an intrinsic dynamo is also a key factor. Recently, it was shown that this dynamo remained active until around 3.7 or 3.6 Gyr ago, possibly twice longer than previously thought [*Milbury et al*., 2012; *Langlais et al*., 2012]. The rate of O and C atoms sputtered from Mars' atmosphere (dark solid line) as calculated by *Leblanc and Johnson* [2002] is plotted in Figure 3 (see *Chassefière and Leblanc* [2004] for explanations of these different mechanisms). This rate was calculated using the flux of incident picked up ions reimpacting Mars' atmosphere from *Luhmann et al*. [1992] who used a simple gas-dynamic approximation of Mars' interaction with the solar wind. In Figure 3, the rate of O atoms (blue dashed line) lost by dissociative recombination (*Luhmann et al*. [1992] and following the corrections suggested by *Jakosky et al*. [1994]) is also plotted as well as the rate of picked up O atoms formed and accelerated by the solar wind outside Mars' gravity (green solid line) as calculated by *Lammer et al*. [2003] and the estimated rate of O and C atoms associated to ionospheric outflows (orange dashed line) calculated by *Ma et al*. [2004]. In that case, we extrapolated the estimates of Mars' present atmospheric escape rates to earlier epochs by a simple exponential relation. The C escaping rate associated to dissociative recombination was also extrapolated to epochs earlier than 2.55 Gyr from *Fox* [2004] estimates. The C pickup ion rate was inferred from the production rate of C atoms by dissociative recombination (considered as the main source of exospheric C atoms). In Figure 3, we also plotted the measured O^+ escaping rate reported by Phobos 2 [*Lundin et al*., 1989]. These authors estimated that around 2.5×10^{25} ions/s were escaping Mars' atmosphere at solar maximum (equivalent to 3 to 4×10^{25} O^+/s based on Mars' ionospheric composition). At solar minimum activity, *Nilsson et al*. [2011] estimated that Mars' O^+ atmospheric loss was equal to $2.0 \pm 0.2 \times 10^{24}$ O^+/s. Based on the atmospheric escape rates displayed in Figure 3, it was then possible to estimate that during the last 4.1 Gyr, up to ~10 mbar of CO_2, and around ~5 m of water were lost to space. By assuming that dynamo cessation occurred 3.6 billion years ago [*Milbury et al*., 2012], these values translate in few mbar of CO_2 and less than 1 m of water. This cumulated loss is clearly dominated by the atmospheric sputtering rate at the earliest epoch of this extrapolation, 4 Gyr ago.

[25] A major progress in the description of Mars' solar wind interaction was obtained thanks to the development of 3-D magnetohydrodynamic model [*Ma et al*., 2004; *Harnett and Winglee*, 2003, and references therein] or 3-D hybrid model [*Brecht and Ferrante*, 1991; *Kallio and Janhunen*, 2002; *Modolo et al*., 2005]. In particular, new and better estimates of the rate of picked up ions reimpacting Mars' atmosphere could be obtained at solar minimum and maximum activities by *Chaufray et al*. [2007] which led to a drastic change in the estimated sputtering rate evolution with time (dark solid line on the right panel). Based on these improved models, new C total escape rates (red dashed line, right panel) were also calculated by *Ma and Nagy* [2007]. Moreover, *Valeille et al*. [2010] published the most complete description of the diurnal, annual, and solar cycle evolutions of the dissociative recombination of the O_2^+ ions in Mars' atmosphere and the associated O escape rates. Such a calculation leads to a much stronger present atmospheric escape (blue dashed line in Figure 3, top right panel) than previously calculated but also a smoother dependency of the escape rate with solar activity. The main evolution from *Chassefière and Leblanc* [2004] and *Chassefière et al*. [2007] derives from the use of a better model of Mars' interaction with the solar wind when describing the fate of the picked up ions. Indeed, in *Luhmann et al*.'s [1992] calculation of the picked up ions fate, an increase of the EUV/UV solar flux implied an increase of the ionization rate and therefore of the picked up ions flux. This increasing flux of picked up ions was then associated with an increase rate of sputtered atmospheric particles. *Luhmann et al*. [1992] concluded that from solar minimum to solar maximum, the sputtering rate increases by a factor of 50. Moreover, *Johnson and Luhmann* [1998] also suggested that this increased rate of sputtered particles from Mars' atmosphere should lead to a denser exosphere and as a consequence to a larger rate of ionization and of picked up ion formation. *Johnson and Luhmann* [1998] concluded that such a feedback could lead to an increase of the sputtering rate by less than a factor of 2, leading to a total increase by 2 orders of magnitude of the sputtered rate from solar minimum to maximum. However, the coupling of exospheric and magnetospheric models realized in *Chaufray et al*. [2007] allows taking consistently into account the feedback of the exosphere on the magnetosphere and vice versa. Such work concluded that the increase of the EUV/UV flux should lead to an increase of the ionization rate but also to the ionospheric pressure that counterbalances the solar wind pressure. As a consequence, an increase of the EUV/UV flux should also lead to the increase of the planetopause altitude (namely, the distance at which the solar wind is stopped). Following this scenario, the newly picked up ions are accelerated further from Mars' atmosphere, and the flux of picked up ions that come back into Mars' atmosphere is significantly decreased with respect to a scenario where the ionospheric pressure is not taken into account. As a conclusion, *Chaufray et al*. [2007] estimated that from solar minimum to solar maximum activities, the sputtering rate was not increasing by more than a factor of 4. In this new scenario, the dissociative recombination of the Martian O_2^+ ions is the major source of neutral atmospheric escape at all epochs back to 3.4 Ga (Figure 3, right panels). Based on these estimates, CL11 and *Chassefière and Leblanc* [2011b] concluded that only ~7 mbar of CO_2 and ~5 m of GEL water could have been lost during the last 4.1 Gyr. These values translate in few mbar of CO_2 and less than 1 m of GEL water if the dynamo ceased later, around 3.6 Gy ago.

[26] It should be pointed, however, that this estimate of cumulated escape loss did not consider the role of solar energetic particle (SEP) event in eroding Mars' atmosphere. It has been observed recently during SEP encounter with Mars a significantly more intense escape rate of Mars' atmosphere [*Edberg et al*., 2010]. Our younger Sun which was probably more active than today, could have induced more atmospheric escape that presently estimated. However, a loss of few tens of mbar of CO_2 and tens of meter of water since 3.6 to 4 Gyr would correspond to an increase of the present escape atmospheric rate by much more than an order of magnitude which is clearly not what is observed during SEP event.

[27] As depicted in this section, our present knowledge of Mars' water atmospheric escape is far from being perfect because of the relatively limited set of measurements obtained so far, the difficulty to extrapolate its modeling to past conditions and the complexity of its description. *Chaufray et al*. [2007] made one of the first attempts to take that complexity into account and taught us how much different could be the results with respect to simpler model, in particular when describing the sputtering effects. The second most quoted process leading to atmospheric escape, dissociative recombination, was the subject of many more recent works which all reached similar conclusions. However, because all these models are based on the same understanding of the thermosphere/ionosphere chemistry (derived from Viking measurements), here again, a lot of caution must be taken. Therefore, without new direct and/or indirect measurements of Mars' atmospheric loss, our knowledge of Mars' past evolution will remain within the range of uncertainties illustrated in Figure 3. Direct measurements would consist in neutral and ion escape rates measured in situ around Mars during a whole Martian year and for different solar activities. Key original indirect measurements of Mars' water escape would be isotopic measurements in the upper atmosphere and exospheric profiles above few hundred kilometers in altitude. As a matter of fact, the Mars Aeronomy and Volatile Evolution mission (MAVEN) mission to Mars, to be launched in 2013, has been conceived to cover most of these measurements [*Jakosky*, 2011]. It should provide us a much better picture of the ion escape rates, of Mars interaction with the solar wind, of Mars' exosphere, and of the isotopic composition of the Martian atmosphere. MAVEN will also probably revolutionize our knowledge of the thermospheric and ionospheric profiles of the neutral and ion densities and temperature during deep-dips campaigns. Indeed, these campaigns will explore the top part of Mars' ionosphere, so far visited only 2 times by the Viking missions in the 70's. This region of Mars is where should occur both dissociative recombination and sputtering the two drivers of Mars' water atmospheric escape.

4. Calculation of the D/H Ratio

[28] The present D/H ratio is the result of thermal escape of hydrogen released by different oxygen loss processes: iron oxidation through serpentinization, sulfur oxidation, and oxygen loss by nonthermal escape. We will assume, according to CL11, that the maximum amount of water consumed by sulfur oxidation is a 10 m thick GEL. According to the results

of section 3, one or a few meters of water have been removed by nonthermal escape since the cessation of the dynamo. In the following, we will assume that the combined effect of sulfur oxidation and oxygen escape has resulted in the loss of a 10 m thick water GEL. This quantity is small, and the exact value of this amount has a little impact on the results.

[29] As we said in section 2, an important parameter of the study is the ratio r between the ingoing number of H_2O molecules and the outgoing number of H_2 molecules in the serpentinization reaction. The value of r, or range of values of r, to be used in the following must fit existing observational and modeling constraints on the magnesium content of Martian olivines, and be such as serpentinization is efficient. For this work, Mg number of 75 has been used (see Table 1). Olivine and pyroxenes may react directly with water (reaction #1) or also react between each other and with H_2O (reactions #2–#4).

[30] The ratio r of ingoing H_2O molecules to outgoing H_2 molecules is reported in the last column of Table 1. This ratio is seven according to the generic serpentinization reaction involving Fo75 (Equation 1 and #1 in Table 1): One H_2 molecule is released for seven H_2O molecules involved in the reaction. As shown in Table 1, this ratio may vary from one reaction to the other one.

[31] Olivines in the Fo70–95 range and pyroxenes in the range En40–95 are also considered (see section A1). According to the analysis presented in section A1, the most likely value of r is seven (Fo75), with an uncertainty in the range from 5 to 10 (Fo70–80), and possibly up to 4–20 (Fo60–Fo85). Values of r in the range from 4 to 20 will therefore be considered.

[32] Considering Fo70 (reactions A5, A21, and A22 in Table A1 of section A1), the average value of r is ~5. Assuming a serpentinization efficiency of 90%, the magnetization is higher than for Fo75 and is associated with an amount of water involved in serpentinization in the range from ~390 m (conservative value, not taking into account ESD with magnetization lower than 1 A/m) to ~650 m (upper value). The thickness of the water GEL contained in the serpentine will be denoted by S in the following. Considering Fo80 (reactions A4, A19, and A20 in Table A1), the average r value is ~8, and S is in the range from 610 m to 1030 m. Note that in this case, the maximum thickness of the required magnetized layer is larger than 40 km. This would imply a thermal gradient in the crust lower than 10 K/km, because serpentinization cannot occur for a temperature larger than ~400°C. We therefore do not take into account the deepest part (>40 km) of the magnetized crust to compute the amount of trapped water. For a magnesium content larger than 80%, the thickness of the serpentinized layer is larger than 50 km, which does not seem realistic for early Mars [see Q09, section 2.1 as well as *McGovern et al.*, 2004; *Grott et al.*, 2011]. Therefore, values of the magnesium content larger than 80% will not be considered any longer in this study. For Fo60 (reactions A6 and A23 in Table A1), S is in the range from 330 m to 550 m], with $r \sim 4$.

[33] The latter calculations are based on the hypothesis that only chemical remanent magnetization (CRM) by serpentinization magnetized the Noachian Martian crust. As discussed later in section 5, other magnetization processes have or may have occurred. Thermoremanent magnetization (TRM) is very likely, especially close to volcanic provinces but also where deeper magmatic intrusions took place. The relative proportion of TRM to CRM is very hard to evaluate. It is also likely that large impacts were associated with magnetization (shock remanent magnetization, SRM) as well as with impact magnetization. The amount of magnetization which disappeared through these events (and through thermal demagnetization after the dynamo cessation) is again difficult to estimate. Our results are thus valid only in the limits of the assumptions we made.

[34] The second parameter of the study is the amount of water w present in the today Martian cryosphere. As developed in section 1, the present inventory of water in surface and close subsurface reservoirs is uncertain, in the range from ~20 m to ~30 m or more (~35 m according to *Christensen* [2006]) in terms of GEL thickness. We will consider in the following values of w in the range from 20 m to 40 m.

[35] The expected value of the D/H ratio due to the combination of O escape, sulfur oxidation and iron oxidation through serpentinization may be written:

$$D/H = (w + 10 + S/r)/w \quad (2)$$

[36] Writing this equation, we assume that deuterium does not escape by thermal escape [*Krasnopolsky*, 2002]. S/r represents the amount of deuterium accumulated due to the thermal escape of the hydrogen released by serpentinization in units of the thickness of a water GEL containing the corresponding amount of deuterium. The amount of deuterium is 10 m, in the same units, resulting from both nonthermal O escape and sulfur oxidation. In this way, $w + 10 + S/r$ is the total amount of deuterium remaining on the planet, whereas the only remaining ^1H is the one contained in the water today present in surface and subsurface reservoirs (w). We assume that the D/H value measured in the atmosphere is representative of the D/H value in the reservoirs exchanging with the atmosphere (polar caps, regolith...).

[37] Some D/H fractionation between water and serpentine is expected. The δD value is in the range from −100‰ to +30‰ depending on the temperature, the type of water (sea, magmatic...) and the water/ rock ratio [*Sakai and Tsutsumi*, 1978]. In the most frequent cases, the serpentine is depleted in deuterium, δD being in the range from ~0 to ~−0.1. Although this effect is small, it has to be taken into account, and equation (2) becomes

$$D/H = (1 + 10/w) + (S/r)[(1\text{-}\delta D)/w] \quad (3)$$

[38] In the following, we will consider for δD the two values 0 and −0.1.

[39] The values of the S/r ratio, taking into account the uncertainty on S, are ~80 m–136 m for Fo60 ($r \sim 4$), ~80 m–135 m for Fo70 ($r \sim 4.9$), ~75 m–125 m for Fo75 ($r \sim 6.5$), and ~70 m–120 m for Fo80 ($r \sim 8.3$). Interestingly, this range only little depends on the magnesium content. It is due to the fact that the amount of magnetite formed through serpentinization, therefore the magnetization of the formed material, is inversely proportional to r. As may be seen on Tables 1 and A1, the number of H_2 atoms formed through serpentinization reactions is closely proportional to the number of magnetite molecules formed through these reactions. The higher r is, the lower the magnetization. The lower the magnetization is, the larger the amount of serpentinized material required to fit the observed magnetization.

Table 2. Values of r (Taken as the Average of Appropriate Chemical Reactions in Tables 1 and A1), Ranges of S and S/r, and Ranges of D/H for Different Amounts of Water Present Today in Reservoirs Exchanging With the Atmosphere, for Various Magnesium Contents of Mafic Rocks[a]

	M (A/m)	T_{max} (km)	T_{ave} (km)	r	S (m)	S/r (m)	D/H for $w = 20$ m	D/H for $w = 30$ m	D/H for $w = 40$ m
Fo60	19.7	24.9	0.99–1.66	4.0	330–550	80–135	5.6–8.4	4.1–5.9	3.3–4.7
Fo70	16.5	29.7	1.18–1.98	4.9	390–650	80–135	5.5–8.1	4.0–5.8	3.2–4.6
Fo75	13.1	37.4	1.49–2.49	6.5	490–820	75–125	5.3–7.8	3.8–5.5	3.1–4.3
Fo80	10.3	47.5	1.84–3.11	8.3	610–1030	70–120	5.2–7.7	3.8–5.5	3.1–4.4

[a]M represents the mean magnetization for a 90% serpentinization. T_{max} is the maximum magnetized thickness as required from the ESD magnetization model. T_{ave} is the average thickness of the magnetized layer, taking or not taking into account those locations where the magnetization is lower than 1 A/m in the starting ESD model. Thicknesses exceeding 40 km are not considered (see text for details).

[40] We will use in the following one single range of 80 m–135 m, representative of all magnesium compositions in the range from 60% to 80%. Above 80%, the thickness of the serpentinized layer is larger than 50 km, which is unrealistic as previously explained. Below 60%, the serpentinization reaction becomes inefficient both thermodynamically and kinetically [*Oze and Sharma*, 2007].

[41] Assuming $\delta D = 0$, the D/H ratio for a present content of water $w = 20$ m is in the range from 5.2 to 8.4. For $w = 30$ m (respectively, 40 m), D/H is in the range from 3.8 to 5.9 (respectively, from 3.1 to 3.7). Assuming $\delta D = -0.1$, the value of the D/H ratio is increased by less than 10%, which does not significantly change the results. Therefore, the present D/H ratio (~5) may be fitted, either with a present amount of water exchanging with the atmosphere of 20 m (that is the content of polar caps) by using conservative estimates of the serpentinized water, or with a present amount of water of 30 m by using upper estimates, without removing regions of low magnetization below the estimated error level. A larger amount of 40 m or more requires additional mechanisms to fractionate hydrogen, since the full range of D/H ratio in this case is below the observed value. Results are summarized in Table 2.

[42] The amount of water trapped in serpentine depends on the magnesium content. The most likely value, using the conservative estimate done for Fo75, is 490 m, with a range of uncertainty from 330 m (conservative estimate for Fo60) to 1030 m (upper estimate for Fo80). A value of 500 m within a factor of 2 is assumed for the discussion. Our results are consistent with a present amount of water exchanging with the atmosphere of 20–30 m. A larger amount cannot be excluded, but, in this case, hydrogen isotopic fractionation would be due only partly to serpentinization (combined with minor oxygen escape and sulfur oxidation contributions), and additional mechanisms would be required.

5. Discussion

[43] The plausibility of serpentinization as the reason for the strong magnetization found mostly in Southern crust is reinforced by independent arguments. Olivine and serpentine were jointly detected in the vicinity of Valles Marineris [*Quantin et al*., 2012], and especially in massive rocks located on its eastern part, where the remanent magnetic field is significantly different from zero [*Purucker et al*., 2000]. These would further argue for a deep-seating alteration process, such as serpentinization. Some of the alteration reactions do produce quartz. This mineral was also identified at the surface of Mars, notably close to Antoniadi crater [*Smith and Bandfield*, 2012]. In this area, quartz-bearing deposits are co-located with other hydrated minerals. While not the main subject of this study, the presence of quartz may therefore be explained by our scenario, as a by-product of serpentinization.

[44] Several limiting factors must be discussed. For estimating the quantity of water trapped below the surface using magnetic field information, we make the assumption that the magnetic field (or the magnetization) has not been altered since it was put into place. CRM associated with serpentinization is very stable, with relaxation time much greater than 100 Myr. There are thus no reasons for an alteration of this magnetization unless one involves exogenic processes such as impact craters and volcanic activity. The crater production rate has been relatively low, and one can estimate that less than 1% of the Martian surface has been affected by impact craters during the last 3 Gy [*Hartmann and Neukum*, 2001]. Volcanic activity remained intense during this period, but this was really locally limited, therefore not likely to affect more than 10% of the Martian surface [*Robbins et al*., 2011]. Our estimate is also not sensitive to serpentinization reactions which took place after the dynamo cessation (not before 3.77 Gy, *Langlais et al*. [2012], and possibly as late as 3.6 Gyr, *Milbury et al*. [2012]). Water is, however, the controlling factor of this alteration process, and it was recently shown that water activity at the surface dramatically stopped around 3.6 Gy ago [*Mangold et al*., 2012], it is expected that most of the serpentinization took place before that epoch. Based on these considerations, our estimate could be seen as a minimum one.

[45] On the other hand, some parts of the inferred magnetization could be related to TRM, i.e., cooling of magnetic material in the presence of an ambient field. Some volcanic structures are associated with lower magnetizations [*Langlais and Purucker*, 2007; *Hood et al*., 2010; *Milbury et al*., 2012] and may be compatible with TRM. Although we cannot rule out this kind of magnetization above or close to volcanic structures, these are spatially limited and should only marginally affect our result, as such thermal magnetization is generally weaker than the chemical one.

[46] The serpentinization scenario proposed by CL11 allows to explain the large observed isotopic fractionation factor of hydrogen. The generally admitted scenario of H fractionation through only escape is clearly not compatible with the low calculated cumulated amount of oxygen lost to space through nonthermal escape since the cessation of the dynamo (the equivalent of less than 1 m thick water GEL). First, the sputtering rate has been greatly overestimated in the last decade in the absence of self-consistent solar wind-ionosphere interaction models (see section 3). Second, the revision of the cessation date of the dynamo has been recently proposed, from 4.1 Gy to 3.6–3.7 Ga (see above), still reducing the calculated

cumulated rate of oxygen escape. Despite uncertainties necessarily affecting our magnetization and hydrogen isotopic fractionation models, the high level of consistency between the two models in terms of amounts of water trapped in serpentine (a 500 m water GEL) makes this hypothesis plausible.

[47] Such a massive episode of serpentinization could have produced huge amounts of methane and then trapped in subsurface clathrates. Methane has been recently discovered in the Martian atmosphere at a typical 10 ppb level [*Krasnopolsky et al*., 2004; *Formisano et al*., 2004; *Mumma et al*., 2009; *Fonti and Marzo*, 2010]. It has been suggested that this methane is produced at depth by serpentinization in crustal hydrothermal systems, then incorporated to the cryosphere under the form of clathrates, and finally released to the atmosphere [*Chassefière and Leblanc*, 2011b; *Mousis et al*., 2013]. If so, methane may be considered as a link of a long-term carbon cycle. This cycle would be progressively damped, with a progressive net removal of CO_2 from the atmosphere to crustal sinks (carbonates—see below—, CO_2 clathrates…). During subsurface magmatic events triggering hydrothermal activity, this crustal CO_2 could be recycled to hot fluids and involved in CH_4 production during serpentinization. Most of this activity would have occurred during Noachian and Hesperian times, but some residual activity could have been maintained until more recent epochs. A total amount of CH_4 equivalent to an atmospheric CO_2 pressure of 0.2–2 bar could have been cycled though the crust through carbonation-serpentinization-methane release, consistently with the present mixing ratio of CH_4 in the atmosphere [*Chassefière and Leblanc*, 2011b; *Mousis et al*., 2013].

[48] The process of serpentinization could have occurred over 500–800 Myr and until the cessation of the Martian core dynamo (which could have occurred as late as 3.6–3.7 Gyr ago), and therefore extended over most of the Noachian. Serpentinization could have been still substantial at late Noachian/early Hesperian. In the present paper, the serpentinized layer is not invoked to explain the crustal dichotomy like in Q09. The key point here is the timing of 1-dynamo, 2-serpentinization, and 3-dichotomy. Our model invokes serpentinization during about 500 to 800 Myr, while a dynamo is active. The thickness calculations in this model attempt to explain the magnetization, and not only the topographical dichotomy, as in Q09. But the results are not inconsistent. Indeed, serpentinization/storage of surface water may have continued after the formation of the 6 km dichotomy, increasing the crustal root rather than its effect on surface (Airy compensation model).

[49] The global scale episode of fissural volcanism which occurred between 3.8 and 3.6 Ga [*Ody et al*., 2013] may have resulted in significant serpentinization. In the same time, the circulation of CO_2-rich hot waters in the subsurface and the deposition of carbonates in crustal cold water pools [CL11] could have triggered the trapping of atmospheric CO_2 in carbonates. The transition from explosive to effusive eruption style occurring at approximately 3.5 Gyr ago [*Robbins et al*., 2011] could also be related to the drastic decrease of water present at the surface and at depth, as explosive regime is generally related to outgassing [*Degruyter et al*., 2012]. The main period of serpentinization could have therefore ended during the early Hesperian. Interestingly, our estimate of the amount of water stored in serpentine (~330–1030 m) is similar to the amount of water required to have formed valley networks from mid-Noachian to early Hesperian (~300–1000 m) [see, e.g., *Lasue et al*., 2013]. We also note that most outflow channels formed during the late Hesperian, possibly after the main serpentinization period. Some of the water present on Mars during the Noachian should therefore not have been converted into serpentine. Although our two independent constraints (crust magnetization, D/H ratio) point toward the same values of the amount of water consumed in serpentinization over the Noachian and early Hesperian, it cannot be excluded that these values are an upper range. But the present work clearly shows that the amount of water stored in serpentine could be quite substantial.

[50] Precipitation of carbonates in subsurface hydrothermal systems could explain the decrease of the CO_2 pressure from the typical 1 bar value at the Noachian down to the present 7 mbar value. As shown in section 3, only a few mbar of CO_2 may have been lost through C nonthermal escape since the cessation of the dynamo. The only alternative is that CO_2 has precipitated as carbonates in crustal hydrothermal systems at the end of the Noachian and during the Hesperian, possibly until present days [*Chassefière and Leblanc*, 2011b; *Lammer et al*., 2013]. Existing observations and modeling are consistent with the occurrence of carbonate precipitations. Carbonates are found in ALH84001 and other SNC meteorites [*Nyquist et al*., 2001]. Magnesium carbonates have been observed at some places at the surface of Mars by the spectro-imager Compact Reconnaissance Imaging Spectrometer for Mars from Mars Reconnaissance Orbiter and by the Spirit Rover [*Ehlmann et al*., 2008; *Morris et al*., 2010; *Niles et al*., 2013]. The observations made by Spirit suggest precipitation from C-rich hydrothermal fluids. Formation of carbonates in the subsurface has also been suggested by geochemical modeling [*Griffith and Shock*, 1995]. The scarcity of carbonates detected from Martian orbit [*Ehlmann et al*., 2008] does not contradict the idea of a long-term carbon cycle involving carbonate deposition. The formation of carbonates in the subsurface at the late Noachian and during the Hesperian is a plausible alternative to the nonthermal escape scenario, unable to explain the loss of hundreds mbar of CO_2 during the last 3 to 4 Gyr.

[51] A possible simultaneous decrease of water at the surface of the planet and carbon dioxide in the atmosphere at the late Noachian/early Hesperian due to enhanced hydrothermal activity in the subsurface, resulting in both massive serpentinization and carbonate precipitation, would deserve further studies. Only little amounts of H_2O and CO_2 have escaped to space since the cessation of the dynamo, implying that significant amounts of volatiles have been trapped in the crust. In the present paper, we have shown that the loss of a ~500 m thick water GEL, within a factor of 2, through serpentinization may explain both the present D/H ratio in the atmosphere and the crustal magnetization of the Southern crust. Understanding the nature and timing of events able to have triggered the trapping of H_2O and CO_2 in the crust at the Noachian/Hesperian transition is a major challenge for future studies of early Mars water and climate evolution.

Appendix A: Additional Serpentinization Reactions

[52] A series of reactions considering olivines in the Fo60–95 range and pyroxenes in the range En40–95 other than those listed in Table 1 are listed in Table A1.

Table A1. Reactions Considered in Addition to Reactions Listed in Table 1 (Q09)

ID	Reactions of Serpentinization[a]	Magnetization (A m^{-1})[b]	$r = H_2O_{in}/H_{2out}$[c]
A1	$30Fo95 + 43H_2O = 15Ch + 1Mt + 12Br + H_2$	2.7	43
A2	$30Fo90 + 41H_2O = 15Ch + 2Mt + 9Br + 2H_2$	5.5	20.5
A3	$30Fo85 + 39H_2O = 15Ch + 3Mt + 6Br + 3H_2$	8.4	13
A4	$30Fo80 + 37H_2O = 15Ch + 4Mt + 3Br + 4H_2$	11.4	9.25
A5	$10Fo70 + 10H_2O = 4Ch + 2Mt + 1En100 + 2H_2$	18.2	5
A6	$15Fo60 + 16H_2O = 6Ch + 4Mt + 3Q + 4H_2$	23.8	4
A7	$15En95 + 19.5H_2O = 9.5Ch + 0.5Mt + 11Q + 0.5H_2$	2.1	39
A8	$15En90 + 19H_2O = 9Ch + 1Mt + 12Q + 1H_2$	4.1	19
A9	$15En85 + 18.5H_2O = 8.5Ch + 1.5Mt + 13Q + 1.5H_2$	6.2	12.3
A10	$15En80 + 18H_2O = 8Ch + 2Mt + 14Q + 2H_2$	8.4	9
A11	$15En75 + 17.5H_2O = 7.5Ch + 2.5Mt + 15Q + 2.5H_2$	10.5	7
A12	$15En70 + 17H_2O = 7Ch + 3Mt + 16Q + 3H_2$	12.7	5.7
A13	$15Fo95 + 2.5En85 + 23.5H_2O = 10Ch + 0.75Mt + 2.75Br + 0.75H_2$	3.4	31.3
A14	$5\ Fo95 + 10En95 + 19.5H_2O = 9.5Ch + 0.5Mt + 6Q + 0.5H_2$	2.2	39
A15	$15Fo90 + 5En85 + 25.5H_2O = 11.5Ch + 1.5Mt + 1\ Br + 2Q + 1.5H_2$	5.8	17
A16	$5Fo90 + 10En90 + 19H_2O = 9Ch + 1Mt + 7Q + 1H_2$	4.5	19
A17	$15Fo85 + 7.5En85 + 41.75H_2O = 12.75Ch + 5.75Mt + 4.5Q + 16.25H_2$	17.6	2.6
A18	$6Fo85 + 6En90 + 15H_2O = 7Ch + 1Mt + 4Q + 1H_2$	6.0	15
A19	$15Fo80 + 6En70 + 24.8H_2O = 10.8Ch + 3.2Mt + 5.4Q + 3.2H_2$	11.9	7.7
A20	$3Fo80 + 3En75 + 7.1\ H_2O = 3.1Ch + 0.9Mt + 2.8Q + 0.9H_2$	10.9	7.9
A21	$5Fo70 + En40 + 6.6H_2O = 2.6Ch + 1.4Mt + 1.8Q + 1.4H_2$	19.4	4.7
A22	$6Fo70 + 3En60 + 10H_2O = 4Ch + 2Mt + 4Q + 2H_2$	17.4	5
A23	$15Fo60 + 15En60 + 32H_2O = 12Ch + 8Mt + 21Q + 8H_2$	20.0	4

[a]Abbreviations: Fo, Forsterite ($(Mg,Fe)2S_iO_4$); Ch, Chrysotile ($Mg_3Si_2O_5(OH)_4$); Mt, Magnetite (Fe_3O_4); Br, Brucite ($Mg(OH)_2$); En, Enstatite ($(Mg,Fe)_2Si_2O_6$); Q, Quartz (SiO_2); Fs, Ferrosillite ($Fe_2Si_2O_6$). Indices in Fo and En correspond to the magnesium content relative to iron (e.g., Fo75 means $(Mg_{0.75}Fe_{0.25})_2SiO_4$).

[b]Magnetization intensities are calculated via volume percentage of magnetite, magnetic susceptibility, and assuming a surface magnetic field during magnetization of 50,000 nT.

[c]Ratio between ingoing H_2O molecules and outgoing H_2 molecules.

[53] The ratio r of ingoing H_2O molecules to outgoing H_2 molecules is reported in the last column. This ratio is quite variable from one reaction to the other and mainly depends on the magnesium content of the olivine or pyroxene. It is of the order of ~20 for reactions involving Fo90, ~10 for Fo80–85, ~7 for Fo75, and ~5 for Fo70. Numbers are similar for pyroxenes in the En70–90 range. A ratio of 7, corresponding to the serpentinization of an olivine with 75% magnesium (average upper mantle value) has been used in CL11. Because olivines with 70% magnesium are abundant at the surface of Mars and easily serpentinizable, reaction A5 may be important, with a ratio of 5. Considering olivine with 60% magnesium, this ratio would be four. Considering a Fo80 composition, observed in some Martian meteorites [*Taylor et al*., 2002], the ratio is ~10, and is ~20 for Fo90. Numbers derived for enstatite are similar.

[54] **Acknowledgments.** We are indebted to the two anonymous reviewers who provided significant help in making the paper clear and self-consistent. EC, FL: support by interdisciplinary CNRS EPOV program. BL: partial support by ANR-08-JCJC-0126-01.

References

Amit, H., U. R. Christensen, and B. Langlais (2011), The influence of degree-1 mantle heterogeneity on the past dynamo of Mars, *Phys. Earth Planet. Inter.*, *189*, 63–79, doi:10.1016/j.pepi.2011.07.008.

Bibring, J.-P., et al. (2006), Global mineralogical and aqueous Mars history derived from OMEGA/Mars express data, *Science*, *312*, 400–404.

Bjoraker, G. L., M. J. Mumma, and H. P. Larson (1989), Isotopic abundance ratios for hydrogen and oxygen in the Martian atmosphere, *Bull. Am. Astron. Soc.*, *21*, 991.

Brecht, S. H., and J. R. Ferrante (1991), Global hybrid of unmagnetized planets: Comparison of Venus and Mars, *J. Geophys. Res.*, *96*, 11209.

Carr, M. (1987), Water on Mars, *Nature*, *326*, 30–35.

Chassefière, E., and F. Leblanc (2004), Mars atmospheric escape and evolution; interaction with the solar wind, *Planet. Space Sci.*, *52*, 1039–1058.

Chassefière, E., and F. Leblanc (2011a), Constraining methane release due to serpentinization by the observed D/H ratio on Mars, *Earth Planet. Sci. Lett.*, *310*, 262–271, doi:10.1016/j.epsl.2011.08.013.

Chassefière, E., and F. Leblanc (2011b), Methane release and the carbon cycle on Mars, *Planet. Space Sci.*, *59*, 207–217.

Chassefière, E., F. Leblanc, and B. Langlais (2007), The combined effects of escape and magnetic field histories at Mars, *Planet. Space Sci.*, *55*, 343–357.

Chaufray, J. Y., R. Modolo, F. Leblanc, G. Chanteur, R. E. Johnson and J. G. Luhmann (2007), Mars solar wind interaction: Formation of the Martian corona and atmospheric loss to space, *J. Geophys. Res.*, *112*, E09009, doi:10.1029/2007JE002915.

Christensen, P. (2006), Water at the poles and in permafrost regions of Mars elements, 2, 151–155.

Clifford, S. M., J. Lasue, E. Heggy, J. Boisson, P. McGovern, and M. D. Max (2010), Depth of the Martian cryosphere: Revised estimates and implications for the existence and detection of subpermafrost groundwater, *J. Geophys. Res.*, *115*, E07001, doi:10.1029/2009JE003462.

Degruyter, W., O. Bachmann, A. Burgisser, and M. Manga (2012), The effects of outgassing on the transition between effusive and explosive silicic eruptions, *Earth Planet. Sci. Lett.*, *349*, 161–170, doi:10.1016/j.epsl.2012.06.056.

Edberg, N. J. T., H. Nilsson, A. O. Williams, M. Lester, S. E. Milan, S. W. H. Cowley, M. Fränz, S. Barabash, and Y. Futaana (2010), Pumping out the atmosphere of Mars through solar wind pressure pulses, *Geophys. Res. Lett.*, *37*, L03107, doi:10.1029/2009GL041814.

Ehlmann, B. L. et al. (2008), Orbital identification of carbonate-bearing rocks on Mars, *Science*, *322*(5909), 1828–1832.

Ehlmann, B. L., et al. (2009), Identification of hydrated silicate minerals on Mars using MRO-CRISM: Geologic context near Nili Fossae and implications for aqueous alteration, *J. Geophys. Res.*, *114*, E00D08, doi:10.1029/2009JE003339.

Fonti, S., and G. A. Marzo (2010), Mapping the methane on Mars, *Astron. Astrophys.*, *512*, A51.

Formisano, V., S. Atreya, T. Encrenaz, N. Ignatiev, and M. Giuranna (2004), Detection of methane in the atmosphere of Mars, *Science*, *306*, 1758–1761.

Fox, J. L. (2004), CO_2^+ dissociative recombination: A source of thermal and nonthermal C on Mars, *J. Geophys. Res.*, *109*, A08306, doi:10.1029/2004JA010514.

Griffith, L. L., and E. L. Shock (1995), A geochemical model for the formation of hydrothermal carbonates on Mars, *Nature*, *377*(6548), 406-408.

Griffith, L. L., and E. L. Shock (1997), Hydrothermal hydration of Martian crust: Illustration via geochemical model calculations, *J. Geophys. Res.*, *102*, 9135–9143.

Grott, M., et al. (2011), Volcanic outgassing of CO_2 and H_2O on Mars, *Earth Planet. Sci. Lett.*, *308*, 391–400.

Harnett, E. M., and R. M. Winglee (2003), The influence of a mini-magnetopause on the magnetic pile-up boundary at Mars, *Geophys. Res. Lett.*, *30*(20), 2074, doi:10.1029/2003GL017852.

Hartmann, W. K., and G. Neukum (2001), Cratering chronology and the evolution of Mars, *Space Sci. Rev.*, *96*, 165–194.

Head, J. W., and S. Pratt (2001), Extensive Hesperian-aged south polar ice sheet on Mars: Evidence for massive melting and retreat, and lateral flow and ponding of meltwater, *J. Geophys. Res.*, *106*, 12275–12300.

Hood, L. L., K. P. Harrison, B. Langlais, R. J. Lillis, F. Poulet, and D. A. Williams (2010), Magnetic anomalies near Apollinaris Patera and the Medusae Fossae Formation in Lucus Planum, Mars, *Icarus*, *208*, doi:10.1016/j.icarus.2010.01.009.

Jakosky, B. N. (2011), The 2013 Mars atmosphere and volatile evolution (MAVEN) mission to Mars, AGU Fall Meeting.

Jakosky, B. M., R. O. Pepin, R. E. Johnson, and J. L. Fox (1994), Mars atmospheric loss and isotopic fractionation by solar-wind-induced sputtering and photochemical escape, *Icarus*, *111*, 271–288.

Johnson, R. E., and J. G. Luhmann (1998), Sputter contribution to the atmospheric corona on Mars, *J. Geophys. Res.*, *103*, 3649, doi:10.1029/97JE03266.

Kallio, E., and P. Janhunen (2002), Ion escape from Mars in a quasi-neutral hybrid model, *J. Geophys. Res.*, *107*(A3), 1035, doi:10.1029/2001JA000090.

Koeppen, W. C., and V. E. Hamilton (2008), Global distribution, composition, and abundance of olivine on the surface of Mars from thermal infrared data, *J. Geophys. Res.*, *113*, E05001, doi:10.1029/2007JE002984.

Krasnopolsky, V. A. (2002), Mars' upper atmosphere and ionosphere at low, medium and high solar activities: Implications for evolution of water, *J. Geophys. Res.*, *107*(E12), 5128, doi:10.1029/2001JE001809.

Krasnopolsky, V. A., J.-P. Maillard, and T. C. Owen (2004), Detection of methane in the Martian atmosphere: Evidence for life?, *Icarus*, *172*, 537–547.

Lammer, H., H. I. M. Lichtenegger, C. Kolb, I. Ribas, E. F. Guinan, R. Abart, and S. J. Bauer (2003), Loss of water from Mars: Implications for the oxidation of the soil, *Icarus*, *165*, 9–25.

Lammer, H., et al. (2013), Outgassing history and escape of the Martian atmosphere and water inventory, *Space Sci. Rev.*, *174*(1–4), 113–154.

Langlais, B., and M. E. Purucker (2007), A polar magnetic paleopole associated with Apollinaris Patera, *Planet. Space Sci.*, *55*, doi:10.1016/j.pss.2006.03.008.

Langlais, B., M. E. Purucker, and M. Mandea (2004), Crustal magnetic field of Mars, *J. Geophys. Res.*, *109*, E02008, doi:10.1029/2003JE002048.

Langlais, B., E. Thebault, E. Ostanciaux, and N. Mandold (2012), A late Martian dynamo cessation time 3.77 Gy ago, 3rd Early Mars Conference, Lake Tahoe, USA, May 2012.

Lasue, J., N. Mangold, E. Hauber, S. Clifford, W. Feldman, O. Gasnault, C. Grima, S. Maurice, and O. Mousis (2013), Quantitative assessments of the Martian hydrosphere, *Space Sci. Rev.*, *174*, 155–212.

Leblanc, F., and R. E. Johnson (2002), Role of molecules in pick-up ion sputtering of the Martian atmosphere, *J. Geophys. Res.*, *107*(E2), 5010, doi:10.1029/2000JE001473.

Liu, S. C., and T. M. Donahue (1976), The regulation of hydrogen and oxygen escape from Mars, *Icarus*, *28*, 231–246.

Longhi, J., E. Knittle, J. R. Holloway, and H. Wänke (1992), The bulk composition, mineralogy and internal structure of Mars, in *Mars* (A93-27852 09–91), edited by H. H. Kieffer, B. M. Jakosky, C. W. Snyder, and M. S. Matthews, pp. 184–208, Univ. of Arizona Press, Tucson and London.

Luhmann, J. G., R. E. Johnson, and M. H. G. Zhang (1992), Evolutionary impact of sputtering of the Martian atmosphere by O^+ pick-up ions, *Geophys. Res. Lett.*, *19*, 2151–2154.

Lundin, R., A. Zakharov, R. Pellinen, H. Borg, B. Hultqvist, N. Pissarenko, E. M. Dubinin, S. Barabash, I. Liede, and H. Koskinen (1989), First measurement of the ionospheric plasma escape from Mars, *Nature*, *341*, 609–612.

Lundin, R., S. Barabash, A. Fedorov, M. Holmström, H. Nilsson, J.-A. Sauvaud, and M. Yamauchi (2008), Solar forcing and planetary ion escape from Mars, *Geophys. Res. Lett.*, *35*, L09203, doi:10.1029/2007GL032884.

Ma, Y.-J., and A. F. Nagy (2007), Ion escape fluxes from Mars, *Geophys. Res. Lett.*, *34*, L08201, doi:10.1029/2006GL029208.

Ma, Y., A. F. Nagy, I. V. Sokolov, and K. C. Hansen (2004), Three-dimensional, multispecies, high spatial resolution MHD studies of the solar wind interaction with Mars, *J. Geophys. Res.*, *109*, A07211, doi:10.1029/2003JA010367.

Malvoisin, B., F. Brunet, J. Carlut, S. Rouméjon, and M. Cannat (2012), Serpentinization of oceanic peridotites: 2. Kinetics and processes of San Carlos olivine hydrothermal alteration, *J. Geophys. Res.*, *117*, B04102, doi:10.1029/2011JB008842.

Mangold, N., A. Adeli, S. Conway, V. Ansan, and B. Langlais (2012), A chronology of early Mars climatic evolution from impact crater degradation, *J. Geophys. Res.*, *117*, E04003, doi:10.1029/2011JE004005.

McCollom, T., and W. Back (2009), Thermodynamic constraints on hydrogen generation during serpentinization of ultramafic rocks, *Geochim. Cosmochim. Acta*, *73*, 856–875.

McGovern, P., S. Solomon, D. Smith, M. Zuber, M. Simons, M. Wieczorek, R. Phillips, G. Neumann, O. Aharonson, and J. Head (2004), Correction to "localized gravity/topography admittance and correlation spectra on Mars: Implications for regional and global evolution", *J. Geophys. Res.*, *109*, E07007, doi:10.1029/2004JE002286.

Meunier, A., S. Petit, B. L. Ehlmann, P. Dudoignon, F. Westall, A. Mas, A. El Albani, and E. Ferrage (2012), Magmatic precipitation as a possible origin of Noachian clays on Mars, *Nature Geosci.*, *5*, doi:10.1038/NGEO1572.

Milbury, C., G. Schubert, C. A. Raymond, S. E. Smrekar, and B. Langlais (2012), The history of Mars' dynamo as revealed by modeling magnetic anomalies near Tyrrhenus Mons and Syrtis Major, *J. Geophys. Res.*, *117*, E10007, doi:10.1029/2012JE004099.

Modolo, R., G. M. Chanteur, E. Dubinin, and A. P. Matthews (2005), Influence of the solar EUV flux on the Martian plasma environment, *Ann. Geophys.*, *23*, 433–444.

Morris, R. V. et al. (2010), Identification of carbonate-rich outcrops on Mars by the Spirit rover, *Science*, *329*, 421–424.

Mouginot, J., A. Pommerol, W. Kofman, P. Beck, B. Schmitt, A. Herique, C. Grima, A. Safaeinili, and J. J. Plaut (2010), The 3–5 MHz global reflectivity map of Mars by MARSIS/Mars Express: Implications for the current inventory of subsurface H_2O, *Icarus*, *210*, doi:10.1016/j.icarus.2010.07.003.

Mousis, O., et al. (2013), Volatile trapping in Martian clathrates, *Space Sci. Rev.*, *174*(1–4), 213–250.

Mumma, M. J., G. L. Villanueva, R. E. Novak, T. Hewagama, B. P. Bonev, M. A. DiSanti, A. M. Mandell, and D. M. Smith (2009), Strong release of methane on Mars in northern summer 2003, *Science*, *323*, 1041–1045.

Mustard, J. F., et al. (2008), Hydrated silicate minerals on Mars observed by the Mars reconnaissance orbiter CRISM instrument, *Nature*, *454*, 305–309.

Niles, P. B., D. C. Catling, G. Berger, E. Chassefière, B. L. Ehlmann, J. R. Michalski, R. Morris, S. W. Ruff, and B. Sutter (2013), Geochemistry of carboantes on Mars: Implications for climate history and nature of aqueous environments, *Space Sci. Rev.*, *174*(1–4), 301–328.

Nilsson, H., N. J. T. Edberg, G. Stenberg, S. Barabash, M. Holmstrom, Y. Futaana, R. Lundin, and A. Fedorov (2011), Heavy ion escape from Mars, influence from solar wind conditions and crustal magnetic fields, *Icarus*, *215*, 475–484.

Nyquist, L. E., D. D. Bogard, C. Y. Shih, A. Greshake, D. Stöffler, and O. Eugster (2001), Ages and geologic histories of Martian meteorites, *Space Sci. Rev.*, *96*, 105–164.

O'Hanley, D. S., and M. D. Dyar (1993), The composition of lizardite 1T and the formation of magnetite in serpentines, *Am. Mineral.*, *78*, 391–404.

O'Hanley, D. S., and M. D. Dyar (1998), The composition of chrysotile and its relation with lizardite, *Can. Mineral.*, *36*, 727–739.

Ody, A., F. Poulet, J.-P. Bibring, D. Loiseau, J. Carter, B. Gondet, and Y. Langevin (2013), Global investigation of olivine on Mars: Insights into crust and mantle composition, *J. Geophys. Res. Planets*, *118*, 1–29, doi:10.1029/2012JE004149.

Oufi, O., M. Cannat, and H. Horen (2002), Magnetic properties of variably serpentinized abyssal peridotites, *J. Geophys. Res.*, *107*(B5), 2095, doi:10.1029/2001JB000549.

Owen, T., J. P. Maillard, C. DeBergh, and B. L. Lutz (1988), Deuterium on Mars: The abundance of HDO and the value of D/H, *Science*, *240*, 1767–1770.

Oze, C., and M. Sharma (2007), Serpentinization and the inorganic synthesis of H_2 in planetary surfaces, *Icarus*, *186*(2), 557–561.

Parker, R. L. (2003), Ideal bodies for Mars magnetics, *J. Geophys. Res.*, *108*(E1), 5006, doi:10.1029/2001JE001760.

Purucker, M. E., D. Ravat, H. Frey, C. Voorhies, T. Sabaka, and M. Acuna (2000), An altitude-normalized magnetic map of Mars and its interpretation, *Geophys. Res. Lett.*, *27*, 2449–2452.

Quantin, C., J. Flahaut, H. Clenet, P. Allemand, and P. Thomas (2012), Composition and structures of the subsurface in the vicinity of Valles Marineris as revealed by central uplifts of impact craters, *Icarus*, *221*(1), 436–452, doi:10.1016/j.icarus.2012.07.031.

Quesnel, Y., C. Sotin, B. Langlais, S. Costin, M. Mandea, M. Gottschalk, and J. Dyment (2009), Serpentinization of the Martian crust during Noachian, *Earth Planet. Sci. Lett.*, *277*, 184–193.

Raymond, S. N., T. Quinn, and J. Lunine (2006), High-resolution simulations of the final assembly of Earth-like planets I. Terrestrial accretion and dynamics, *Icarus*, *183*, 265–282.

Robbins, S. J., G. Di Achille, and B. M. Hynek (2011), The volcanic history of Mars: High-resolution crater-based studies of the calderas of 20 volcanoes, *Icarus*, *211*(2), 1179–1203.

Sakai, H., and M. Tsutsumi (1978), D/H fractionation factors between serpentine and water at 100° to 500°C and 2000 bar water pressure, and the D/H ratios of natural serpentines, *Earth Planet. Sci. Lett.*, *40*, 231–242.

Smith, M. R., and J. L. Bandfield (2012), Geology of quartz and hydrated silica-bearing deposits near Antoniadi Crater, Mars, *J. Geophys. Res.*, *117*, E06007, doi:10.1029/2011JE004038.

Smith, D. E., et al. (2001), Mars orbiter laser altimeter: Experiment summary after the first year of global mapping of Mars, *J. Geophys. Res.*, *106*, 23689–23722.

Taylor, L. A., et al. (2002), Martian meteorite Dhofar 019: A new shergottite, *Meteor. Planet. Sci.*, *37*, 1107–1128.

Valeille, A., S. W. Bougher, V. Tenishev, M. R. Combi, and A. F. Nagy (2010), Water loss and evolution of the upper atmosphere and exosphere over Martian history, *Icarus*, *206*, 28–39.